Celal Bayar University Journal of Science

A Numerical Investigation into the Thermohydraulic Performance of a Spiral Triangle Solar Air Heater

Seyed Mahdi Taheri Mousavi[1]*

[1]Mechanical Engineering Department, Doğuş University, 34775 Istanbul, Türkiye
* smousavi@dogus.edu.tr
* Orcid No: 0000-0003-1624-0757

Received: July 9, 2025
Accepted: October 19, 2025
DOI: 10.18466/cbayarfbe.1738451

Abstract

In the present study, the thermohydraulic performance of the solar air heater with a triangular absorber plate is numerically investigated. Five various configurations of the absorber plate depend on the number of passageways that were conducted to find the optimum number of passageways. The mass flow rate was chosen between 0.0078 kg/s and 0.0758 kg/s, with an interval of 0.0068 kg/s. The surface area of the collector and bed height were 1 m² and 0.08 m, respectively. The distances between the passageways were chosen as 0.21 m, 0.15 m, 0.11 m, 0.084 m, and 0.073 m, respectively, at two, three, four, five, and six passageways. The numerical analysis was carried out using the ANSYS-FLUENT 2024 R2 solver. The highest effective efficiency, thermal efficiency, and outlet temperature were calculated under different operating conditions. The maximum effective efficiency of 75.4% was achieved at a middle of the range of passageway and mass flow rate, respectively, of three and 0.0418 kg/s. The thermal efficiency reached a peak value of 94.2% at the highest mass flow rate of 0.0758 kg/s with five passageways, however, the effective efficiency reduced to 0% because of the significant growth in pressure drop. Therefore, for arrangements with more than four passageways, mass flow rates beyond 0.0350 kg/s are not suggested.

Keywords: Air passageways, CFD, Effective efficiency, Solar air heater, Thermal efficiency

1. Introduction

Global energy consumption continues to be on the rise as the current population seeks an improved standard of living. For decades, fossil fuels have been exploited as the principal energy source; however, their use increases significant environmental issues. In addition, the sources of fossil fuel are limited and are gradually diminishing. Solar energy, as a kind of renewable energy source, appears as a particularly viable method due to its plentiful, free, and eco-friendly characteristics compared to fossil fuel [1].

Solar air heaters (SAH) are utilized in several applications, such as space heating, drying of agricultural products, water heating, and industrial drying (i.e., paper mills, bricks) [2,3]. Solar heating can be divided into several categories, including those based on the fluid used: SAH and solar water heater. SAHs consist of a transparent cover plate to transparent solar rays, a black-colored absorber plate to absorb solar rays, and a collector casing to capture air inside the SAH, where air with a lower temperature enters, gets heated, and leaves at a high temperature. Conventional SAHs have low conversion thermal efficiency attributed to insufficient heat transfer between the absorber plate and air, compelling modifications to increase heat transfer and consequently improve thermal performance [4].

Different solution methods have been used, such as experimental [5], theoretical [6], and numerical [7,8]. Several methods have been conducted to improve the thermal performance of SAH, which includes increasing the airflow passes [9]. Kumar et al. [10] show that a curved double-pass SAH improved the thermal performance of SAH compared to the single SAH. Raj et al. [11] used an asymmetric channel flow configuration in a double-pass SAH. The experimental results showed that the daily thermal efficiency of the modified SAH was 20% and 41% at the mass flow rates of 0.02 kg/s and 0.03 kg/s, respectively. Heydari and Mesgarpour [12] experimentally and numerically investigated the effect of the helical triangular channeling flow passageway on the thermal performance of a SAH. The results showed that the thermal efficiency of the double-pass helical

channeling increased 14.7% compared to the single-pass SAH.

The amount of heat transfer from the absorber plate to air could be increased by increasing the number of air passageways inside SAH due to raising the time duration for heat transfer. The air channels in SAH are primarily designed as serpentine passageways [13]. While serpentine SAHs significantly improve the thermal performance, the 180° turns at the end of each baffle generate separation vortices, which decrease the convective heat transfer coefficient between the absorber plate and the air flow. Jia et al. [14] show that reducing the turning angle to 90° can improve thermal performance. Jia et al. [15] studied the effect of various number of passageways (ranging from 1 to 8) on the thermohydraulic of the sperial SAH, and observed that the optimal configuration was achieved with two passageways. Jia et al. [16] investigated the effect of various baffle geometries at the turning region, including right-angle spirals, arc spirals, arc spirals with rectangular holes, and rectangular-hole spirals. The numerical results showed that the sperial SAH with right-angle turnings combined with rectangular holes exhibited the best thermal performance compared to the other configurations.

In the current study, the number of turnings decreased to 60°, which was to introduce a novel design called a triangular solar air heater (TSAH). ANSYS-FLUENT 2024 R2 solver is used to investigate the effect of the number of passageways and the mass flow rates on the thermal performance of the TSAH.

2. Numerical procedure

In the current study, the effect of passageways and mass flow rates on the thermal performance of TSAH is investigated by a three-dimensional numerical simulation utilizing the ANSYS-FLUENT 2024 R2 solver.

The length of the equatorial triangle was 1.52 m, and therefore the surface area was 1 m². Figure 2 shows the shematic view of the TSAH with four passageways. The distance of the channels for air passageway was 0.21 m, 0.15 m, 0.11 m, 0.84 m, and 0.73 m, respectively, at two, three, four, five, and six passageways (Figure 3(a-e)). The passageways were implemented by using baffles to find the best configuration. The air is driven to the collector by a rectangular channel with a width of distance between the baffles and a height of 0.08 m, which is constant for all case studies. The heated air was depleted from the collector via a triangular duct. The length of inlet and exit channels is arranged as $10D_h$ to obtain a fully developed flow. The materials for the cover plate, baffles, absorber plate, and insulation were selected as glass, aluminum, aluminum, and wood, respectively, and their thermophysical properties are listed in Table 1.

Table 1. Thermophsical properties of air and materials.

	Specific Heat (J/kg.K)	**Density (kg/m^3)**	**Thermal conductivity (W/m.K)**
Aluminum	871	2719	202.4
Glass	840	2500	0.76
Wood	1250	120	0.04
Air	1006	1.225	0.0242

The computational domain was discretized using an unstructured mesh with tetrahedra, and a number of the element sizes were 0.003 m, 0.005 m, and 0.005 m at the collector, entrance, and exit bodies, respectively. The mesh independence studies were performed to ensure that numerical results were independent of the mesh sizes. Several numbers of meshes were selected until the outlet temperature was in an acceptable tolerance of 0.001 (Figure1). The inflation layer was employed near the walls (cover plate, absorber plate, and baffles) to accurately solve the velocity and temperature gradients.

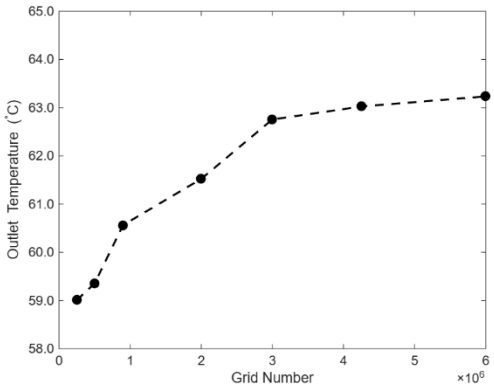


Figure 1.the variation of outlet temperature versus grid numberfor the TSAH with three passageways.

The numerical method is based on solving continuity, Navier Stokes, and energy equations for the 3-dimensional computational domain. The following assumptions were accepted:

Celal Bayar University Journal of Science
Volume 22, Issue 1, 2026, p 1-9
Doi: 10.18466/cbayarfbe.1738451

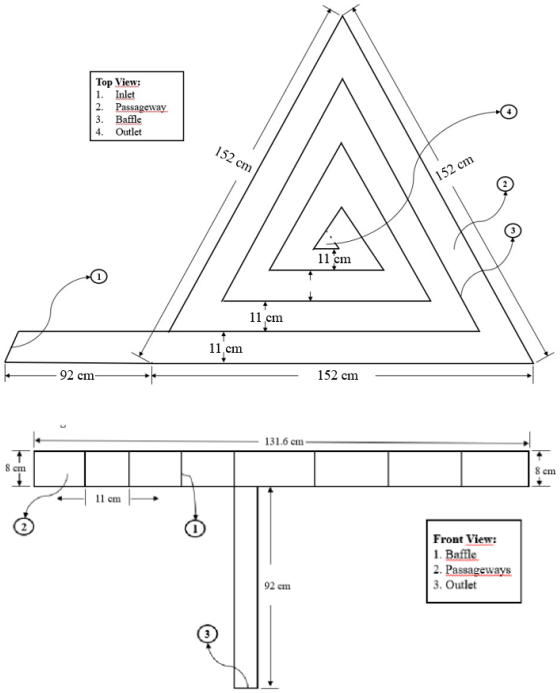


Figure 2. Schematic of a TSAH with four passageways.

- The flow was incompressible and in a steady state.
- The thermodynamic and thermophysical properties were assumed to be constant and did not vary with temperature throughout the solution.

The continuity equation,

$$divV = 0 \quad (\mathbf{1})$$

The momentum equations,

$$div(u\vec{V}) = -\frac{1}{\rho}\frac{\partial p}{\partial x} + \nu div(\nabla u) \quad (\mathbf{2})$$

$$div(v\vec{V}) = -\frac{1}{\rho}\frac{\partial p}{\partial y} + \nu div(\nabla v) \quad (\mathbf{3})$$

$$div(w\vec{V}) = -\frac{1}{\rho}\frac{\partial p}{\partial z} + \nu div(\nabla w) \quad (\mathbf{4})$$

Energy equation,

$$div(T\vec{V}) = \alpha div(\nabla T) + S_s \quad (\mathbf{5})$$

where,

α= thermal diffusivity.
S_s=solar radiation source term, which is calculated by DO model.

A finite volume method was used to discretize the governing equations. The SST K − ω was used for solve the turbulent air flow. The SIMPLE and Second-order upwind scheme models were applied, respectively, for pressure-velocity coupling and discretization of the convection effect to ensure numerical accuracy. The convergence criteria for convergence of all governing equations were selected to be less than 10^{-6}.

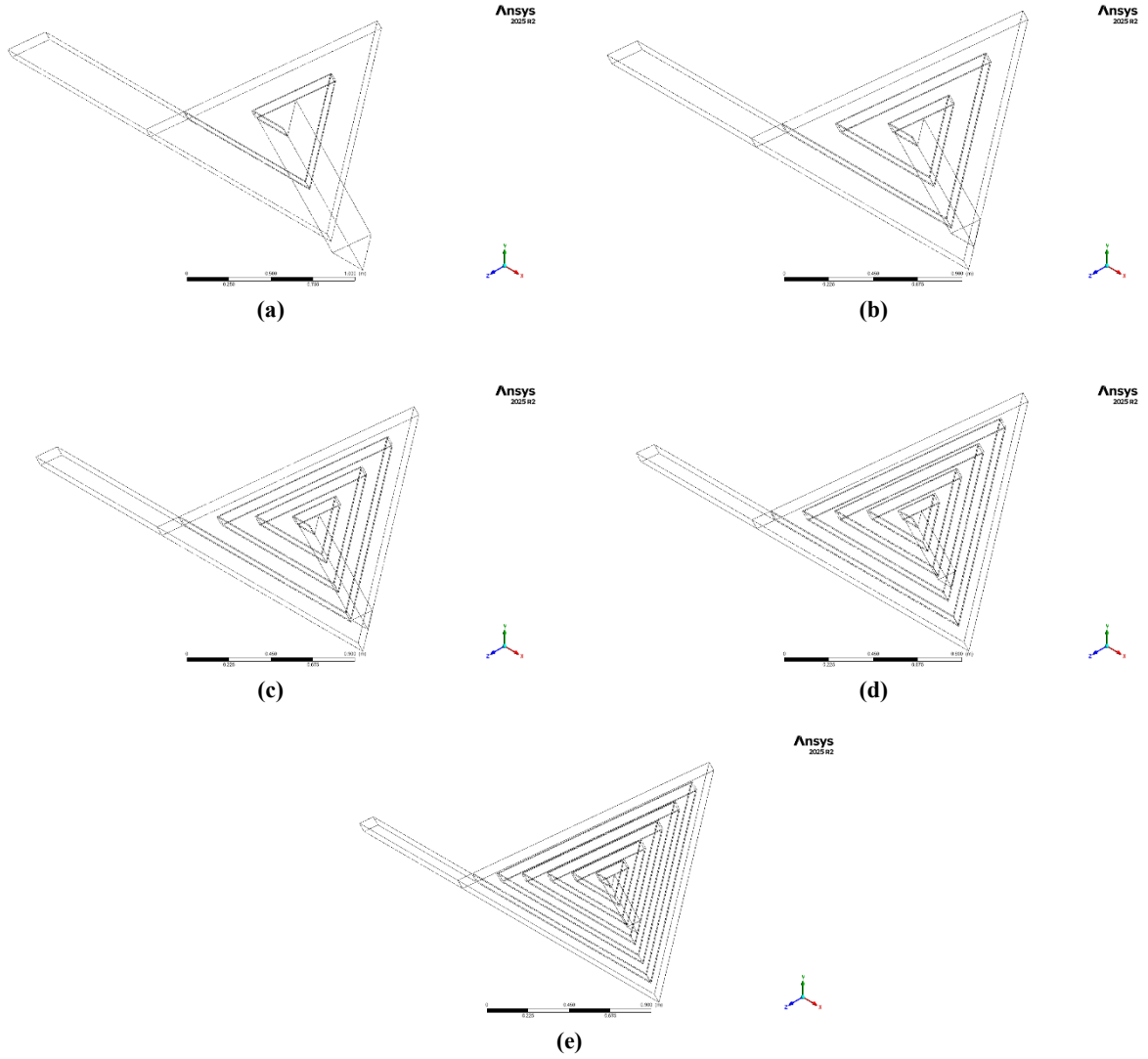


Figure 3. Top view of (a) two Passageways TSAH, (a) three Passageways TSAH, (a) four Passageways TSAH, (a) five Passageways TSAH, and (a) six Passageways TSAH.

The solar energy was applied as the source of energy for the TSAH using the Solar Load-Discrete Ordinate (DO) model. Solar Ray Tracing was used to give the orientation coordinates, time of day, and weather conditions. The latitude, longitude, and time zone were arranged for Istanbul/Turkey. The calculated solar radiation by the Solar Load model is applied to TSAH as the source of heat. The numerical results show that the solar intensity for TSAH with two, three, four, five, and six passageways was 897 W/m², 869 W/m², 845 W/m², 824 W/m², and 823 W/m², respectively. Three main boundary conditions used throughout this numerical study are shown in Table 2.

Table 2. Boundary condition of the computational domain for the TSAH.

Surface	**Boundary Condition**	**Description**		
		Momentum	**Thermal**	**Radiation**
Entrance	Mass Flow Inlet	Mass flow rates arranged between 0.001 kg/s and 0.048kg/s	20.85℃	No participation in Solar Ray Tracing
Absorber Plate	Wall	No Slip Condition	Heat flux=0	Opaque- participation in Solar Ray Tracing, absorptivity of 0.96

Glass Cover	Wall	No Slip Condition	Mixed (Convection and radiation)	Semi-transparent, Transmissivity of 0.92
Baffles	Wall	No Slip Condition	Heat flux=0	Opaque- participation in Solar Ray Tracing, absorptivity of 0.96
Exit	Outlet	Gauge pressure of 0	20.85℃	No participation in Solar Ray Tracing
Others	Wall	No Slip Condition	Heat flux=0	No participation in Solar Ray Tracing

The instantaneous thermal efficiency of the TSAH shows the conversion ratio of the desired output energy to required input energy, which can be calculated by

$$\eta_{th} = \frac{\dot{m}c_p(T_{out} - T_{in})}{IA} \quad (6)$$

where,

$\dot{m}$ = mass flow rate
c_p= specific heat capacity
T_{out}= outlet temperature
T_{in}= inlet temperature
I = solar intensity
A = absorber plate area of the TSAH

Effective efficiency could be utilized to calculate the effect of the passageways within the TSAH by the following equation:

$$\eta_{eff} = \frac{\dot{m}c_p(T_{out} - T_{in}) - \frac{P_f}{C}}{IA} \quad (7)$$

where,

C= conversion constant, which could be used to estimate the overall efficiency of the conversion of thermal energy to mechanical energy and is 0.18 [17].
P_f= power consumed by the fan to pressurize the air to flow across the passageways is defined as

$$P_f = \dot{V}\Delta P \quad (8)$$

where,

$\dot{V}$ = volumetric flow rate
ΔP=pressure drop of the working fluid across the TSAH due to the mirror and major losses, which were calculated by the solver between the inlet and outlet at the area-weighted average.

2. Results and Discussion

The air is driven from a rectangular duct embedded on one of the lateral sides of the TSAH and, after absorbing heat from the absorber plate, discharged to the outside via a triangular duct installed at the nearly center of the absorber plate. Numerical results show that pressure drop within the TSAH strongly depends on the number of passageways at the identical mass flow rate, as illustrated by Figure 4. The lowest pressure drop was achieved at the lowest mass flow rate and passageways of 1.05 Pa, while the maximum pressure drop was achieved at the highest mass flow rate and passageways of 3900 Pa.

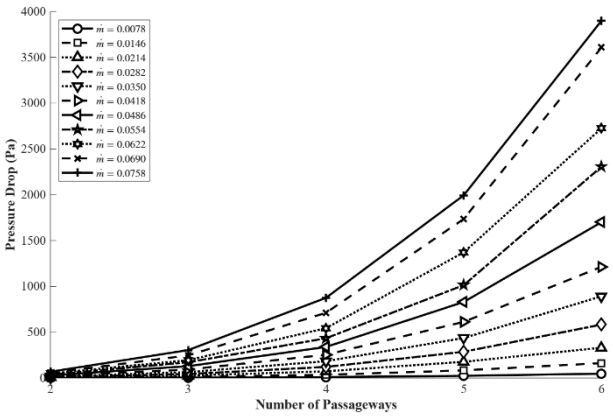


Figure 4. The variation of pressure drops in TSAH with the number of passageways and mass flow rates.

The variation of the temperature difference between the inlet (20.8℃) and outlet of TSAH, which has a significant influence on the thermal performance of TSAH, with the number of the passageways and mass flow rate, is illustrated in Figure 5. Results show that the temperature difference is increased by increasing the passageways and decreased by raising the mass flow rate. The maximum temperature difference was achieved at 45.8°C, where the outlet temperature was 66.7°C, at passageway number 6 and the mass flow rate of 0.0078 kg/s. Figure shows the temperature contours at the absorber plate for the TSAH with 3 passageways.

Celal Bayar University Journal of Science
Volume 22, Issue 1, 2026, p 1-9
Doi: 10.18466/cbayarfbe.1738451

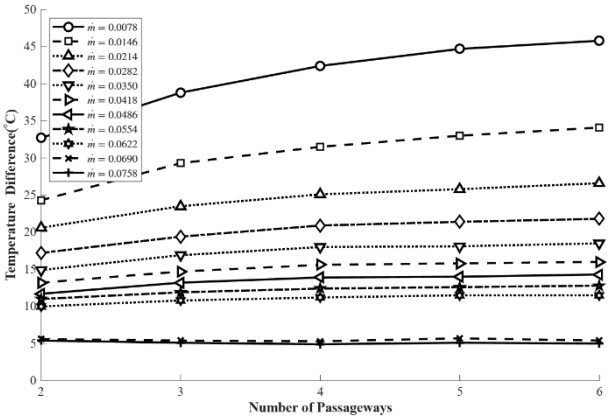
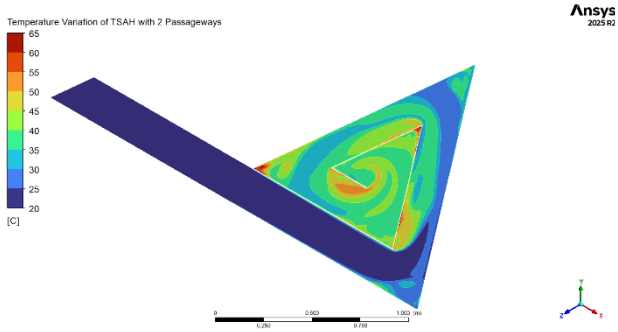


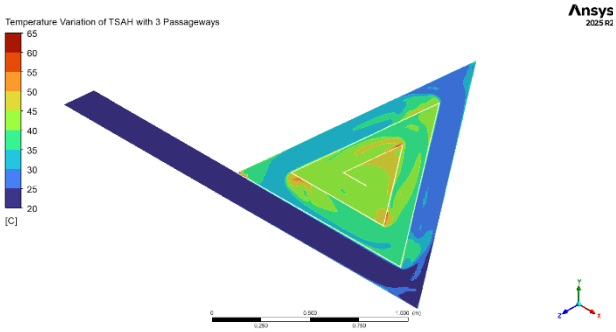
Figure 5. The variation of temperature differences between the inlet and outlet with the number of passageways and mass flow rates.

Figure 6 (a-e) shows the contours of the temperature distribution at a plane constructed between the absorber plate and glass cover and the mass flow rate of 0.0214 kg/s. The plot shows that the temperature of the absorber plate in the first regions of the passageways decreases significantly due to heat transferred from the absorber plate. While at the passageways near the exit, the temperature of the absorber plate remained high since the air is heated through the previous passageways and heat transferred from the absorber plate is decreased. In addition, due to generated vortexes at the turning regions, the heat transferred to air is significantly raised.

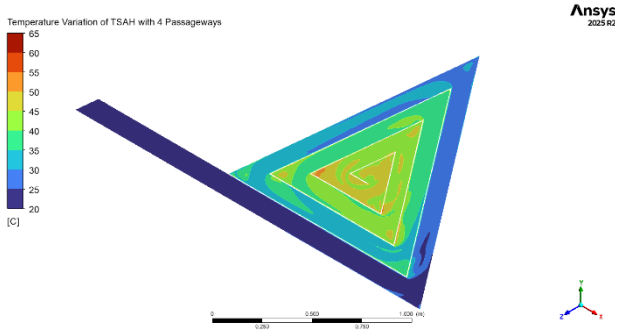
Figure 7 (a-e) illustrates the velocity variations in a TSAH as the number of passageways raises from 2 to 6. With an increase in the number of passageways, the highest velocity of the air stream raises notably (from 2.27 m/s for TSAH with 2 passageways to 8.26 m/s for the TSAH with 6 passageways). The growth results due to reduction in the cross-sectional area for flow in each passage, requiring an increment velocity to keep a constant mass flow rate. The pattern of the flow changes from large, central recirculation regions and remarkable flow separations in broad corners (dark blue zones in the case of passways 2 and 3) to more smooth flow in narrower (passways 4, 5 and 6). By increasing the velocity in the higher-passageway configurations (4, 5, and 6) shows a potential enhancement in heat transfer credited to a higher Reynolds number and raised turbulence. However, this increment in flow resistance will simultaneously lead to a significant growth in pressure drop and the fan power required, results a reduction in effective efficiency.



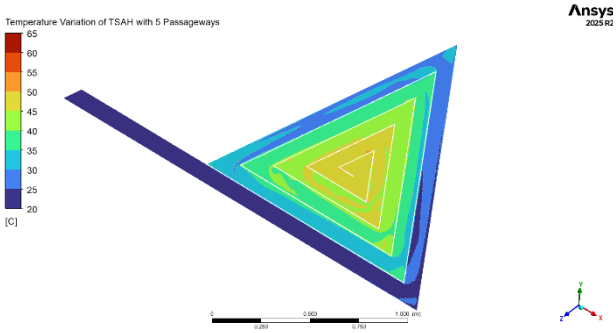
(a)



(b)

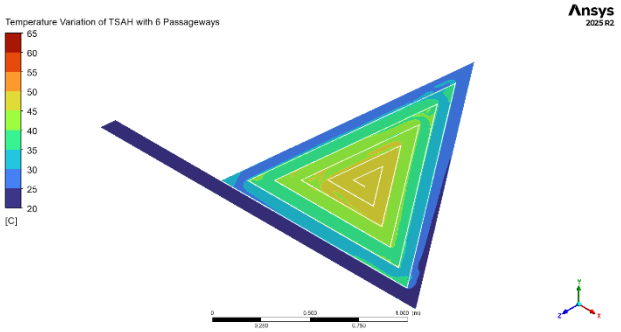


(c)



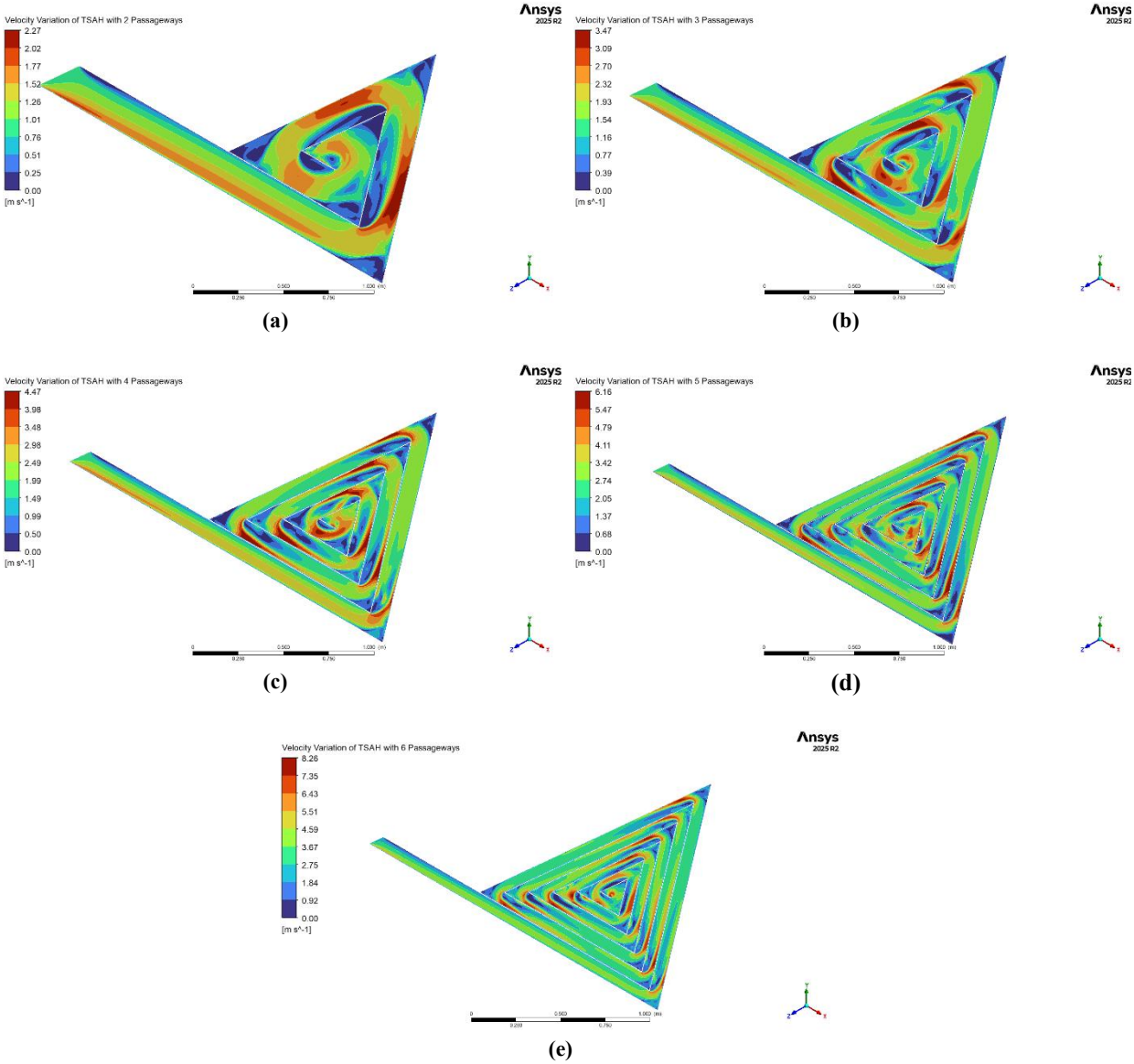
(d)

Celal Bayar University Journal of Science
Volume 22, Issue 1, 2026, p 1-9
Doi: 10.18466/cbayarfbe.1738451



(e)

Figure 6. Contours of temperature variation at the center of the TSAH for different passageways with the mass flow rate of 0.0214 kg/s.



(a) **(b)** **(c)** **(d)** **(e)**

Figure 7. Contours of velocity variation at the center of the TSAH for different passageways with the mass flow rate of 0.0214 kg/s.

Celal Bayar University Journal of Science
Volume 22, Issue 1, 2026, p 1-9
Doi: 10.18466/cbayarfbe.1738451

The variation of thermal efficiency with the number of passageways and mass flow rate is illustrated in Figure 6. The numerical results indicate that thermal efficiency rises consistently with an increase in both the number of the passageways and the mass flow rate. By raising the mass flow rate, more working fluid has the opportunity to contact the absorber plate, boosting the convective heat transfer and improving thermal efficiency. Also, the numerical achievements show that raising the number of passageways leads to higher heat transfer areas and better air circulation and consequently raises the thermal performance. For instance, among the results for various mass flow rates, at a mass flow rate of 0.0078 kg/s, the lowest mass flow rate, the thermal efficiency rises from 29.8 % with 2 passageways in TSAH to 46.4% with 6 passageways. The maximum thermal efficiency achieved is 95.8 % at a mass flow rate of 0.0758 kg/s, where 6 passageways were utilized in TSAH.

The effect of the pressure drop due to the increase in the number of passageways could be measured by effective efficiency. Whereas thermal efficiency takes advantage of raising the number of passageways and mass flow rate, the increment in power consumed by the fan decreases the overall performance, which could be calculated via effective efficiency as illustrated in Figure 7. The results obtained from the numerical method show that except for the lowest value of the passageways (two), where an increase in the effective efficiency of the TSAH was achieved with an increase in the mass flow rate, in the rest of the TSAH with a number of passageways higher than two air paths, an increase was obtained in the effective efficiency with an increase in the mass flow rate up to a point unique to the TSAH, after which a decrease in the effective efficiency was achieved with an increase in the mass flow rate. This peak point occurs in the TSAH with passageways of three, four, five, and six at mass flow rates of 0.0554 kg/s, 0.0418 kg/s, 0.0282 kg/s, and 0.0282 kg/s, respectively.

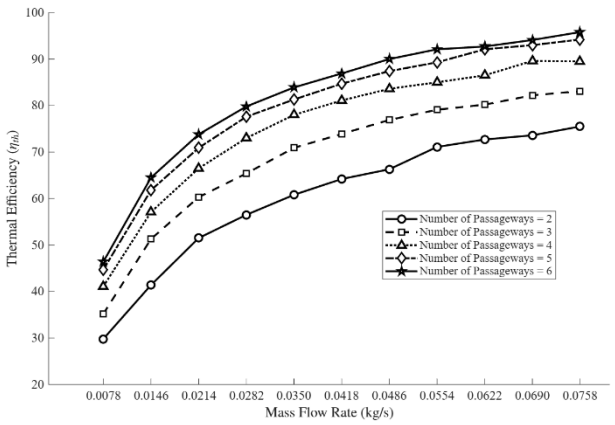


Figure 6. The variation of thermal efficiency by mass flow rates and number of passageways of TSAH.

II.

III.

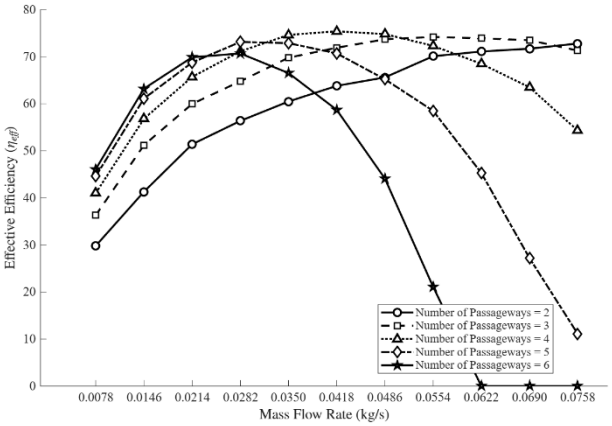


Figure 7. The variation of effective efficiency by mass flow rates and number of passageways of TSAH.

The results of the outlet temperature and thermal efficiency for TSAH with five passageways and a mass flow rate of 0.0214 kg/s are compared with the experimental study conducted by Jia et al. [1]. The experimental study was conducted on the spiral rectangular SAH with five passageways. The comparing is tabulated in Table 3. The inlet temperature for both studies was selected as 20.85℃. The comparison shows an improvement in the thermal performance of the TSAH in comparison to the spiral rectangular SAH.

Table 3. Comparison between the TSAH with spiral rectangular SAH.

Quantity	Spiral rectangular study (Experimental)	Present study (Numerical)
T_{out}	42.5℃	46.64℃
η_{th}	57%	70.9%

3. Conclusion

The numerical results indicate that the thermal efficiency of the TSAH proportionally depends on the mass flow and number of the passageways, and by increasing both, thermal efficiency would be increased. Whereas effective efficiency was achieved at lower mass flow rates and lower passageways due to low power consumed by the fan. The comparison between the present SAH and the spiral rectangular SAH with identical operating conditions shows that outlet temperature and thermal efficiency improved by 9.74% and 24.36%, respectively. Some of the conclusions are listed below:

The maximum temperature difference between the inlet and outlet of TSAH was achieved at SAH with the highest number of both mass flow rate and the number of passageways.
Pressure drop was strongly associated with the number of the passageways and mass flow rate.
The thermohydraulic performance of the TSAH revealed a trade-off between the amount of mass flow rate and

number of passageways. The optimum configuration was achieved with three passageways TSAH. While increasing the mass flow rate can increase the thermal efficiency (up to 95% for six passageways at the highest mass flow rate), a further rise in the number of passageways becomes counterproductive. This is because the effective efficiency reduces drastically (attaing 0% for six passageways at maximum mass flow rate) owing to the considerable increase in power consumption by fan required to overcome the elevated pressure drop inside the TSAH.

Acknowledgement

I gratefully acknowledge Doğuş University for providing access to their workstation, which was used to perform the CFD analysis.

Author's Contributions

Seyed Mahdi Taheri Mousavi: Conceived and designed the study, conducted the numerical simulations and data analysis, interpreted the results, and wrote the manuscript.

Ethics

There are no ethical issues after the publication of this manuscript.

References

[1]. Chaurasia S, Goel V, Debbarma A. Impact of hybrid roughness geometry on heat transfer augmentation in solar air heater: A review. Solar Energy. 2023;255(November 2022):435–59. Available from: https://doi.org/10.1016/j.solener.2023.02.052.

[2]. Yadav AS, Shrivastava V, Sharma A, Dwivedi MK. Numerical simulation and CFD-based correlations for artificially roughened solar air heater. Materials Today: Proceedings. 2021;47(xxxx):2685–93. Available from: https://doi.org/10.1016/j.matpr.2021.02.759.

[3]. Kabeel AE, Hamed MH, Omara ZM, Kandeal AW. Solar air heaters: Design configurations, improvement methods and applications – A detailed review. Renewable and Sustainable Energy Reviews. 2017;70(November):1189–206.

[4]. Soliman AS, Cheng P, Sultan AA, Abdelrehim O, Sultan MA. A new design of a bifacial solar air heater with PCM. Thermal Science and Engineering Progress. 2025;59(February):103380. Available from: https://doi.org/10.1016/j.tsep.2025.103380.

[5]. Promvonge P, Skullong S. Thermal characteristics in solar air duct with V-shaped flapped-baffles and chamfered-grooves. International Journal of Heat and Mass Transfer. 2021;172:121220. Available from: https://doi.org/10.1016/j.ijheatmasstransfer.2021.121220.

[6]. Ammari HD. A mathematical model of thermal performance of a solar air heater with slats. Renewable Energy. 2003;28(10):1597–615.

[7]. Boulemtafes-Boukadoum A, Benzaoui A. CFD based analysis of heat transfer enhancement in solar air heater provided with transverse rectangular ribs. Energy Procedia. 2014;50:761–72. Available from: http://dx.doi.org/10.1016/j.egypro.2014.06.094.

[8]. Jin D, Zhang M, Wang P, Xu S. Numerical investigation of heat transfer and fluid flow in a solar air heater duct with multi V-shaped ribs on the absorber plate. Energy. 2015;89:178–90. Available from: http://dx.doi.org/10.1016/j.energy.2015.07.069.

[9]. Chamoli S, Chauhan R, Thakur NS, Saini JS. A review of the performance of double pass solar air heater. Renewable and Sustainable Energy Reviews. 2012;16(1):481–92. Available from: http://dx.doi.org/10.1016/j.rser.2011.08.012.

[10]. Kumar A, Akshayveer, Singh AP, Singh OP. Efficient designs of double-pass curved solar air heaters. Renewable Energy [Internet]. 2020;160:1105–18. Available from: https://doi.org/10.1016/j.renene.2020.06.115.

[11]. Raj AK, Kunal G, Srinivas M, Jayaraj S. Performance analysis of a double-pass solar air heater system with asymmetric channel flow passages. Journal of Thermal Analysis and Calorimetry [Internet]. 2019;136(1):21–38. Available from: https://doi.org/10.1007/s10973-018-7762-1.

[12]. Heydari A, Mesgarpour M. Experimental analysis and numerical modeling of solar air heater with helical flow path. Solar Energy. 2018;162(January):278–88. Available from: https://doi.org/10.1016/j.solener.2018.01.030.

[13]. Ameri, Mehran, Reza Sardari, and Hadi Farzan. "Thermal performance of a V-Corrugated serpentine solar air heater with integrated PCM: A comparative experimental study." Renewable Energy 171 (2021): 391-400.

[14]. Jia B, Liu F, Wang D. Experimental study on the performance of spiral solar air heater. Solar Energy. 2019;182(September 2018):16–21. Available from: https://doi.org/10.1016/j.solener.2019.02.033.

[15]. Jia, Binguang, et al. "Influence on thermal performance of spiral solar air heater with longitudinal baffles." Solar Energy 225 (2021): 969-977.

[16]. Jia, Binguang, et al. "Optimizing structure of baffles on thermal performance of spiral solar air heaters." Solar Energy 224 (2021): 757-764.

[17]. Cortés A, Piacentini R. Improvement of the efficiency of a bare solar collector by means of turbulence promoters. Applied Energy. 1990;36(4):253–61.